



## Petrology and origin of amoeboid olivine aggregates in CR chondrites

Michael K. WEISBERG,<sup>1,2\*</sup> Harold C. CONNOLLY, JR.,<sup>1,2,3</sup> and Denton S. EBEL<sup>2</sup>

<sup>1</sup>Department of Physical Sciences, Kingsborough College and Graduate School of the City University of New York, 2001 Oriental Boulevard, Brooklyn, New York 11235, USA

<sup>2</sup>Department of Earth and Planetary Sciences, American Museum of Natural History, New York, New York 10024, USA

<sup>3</sup>Department of Geological Sciences, Rutgers University, Piscataway, New Jersey 08854, USA

\*Corresponding author. E-mail: [mkweisberg@kbcc.cuny.edu](mailto:mkweisberg@kbcc.cuny.edu)

(Received 18 September 2003; revision accepted 28 July 2004)

---

**Abstract**—Amoeboid olivine aggregates (AOAs) are irregularly shaped, fine-grained aggregates of olivine and Ca, Al-rich minerals and are important primitive components of CR chondrites. The AOAs in CR chondrites contain FeNi metal, and some AOAs contain Mn-rich forsterite with up to 0.7 MnO and Mn:Fe ratios greater than one. Additionally, AOAs in the CR chondrites do not contain secondary phases (nepheline and fayalitic olivine) that are found in AOAs in some CV chondrites. The AOAs in CR chondrites record a complex petrogenetic history that included nebular gas-solid condensation, reaction of minerals with the nebular gas, small degrees of melting, and sintering of the assemblage. A condensation origin for the Mn-rich forsterite is proposed. The Mn-rich forsterite found in IDPs, unequilibrated ordinary chondrite matrix, and AOAs in CR chondrites may have had a similar origin.

A type A calcium, aluminum-rich inclusion (CAI) with an AOA attached to its Wark-Lovering rim is also described. This discovery reveals a temporal relationship between AOAs and type A inclusions. Additionally, a thin layer of forsterite is present as part of the Wark-Lovering rim, revealing the crystallization of olivine at the end stages of the Wark-Lovering rim formation. The Ca, Al-rich nodules in the AOAs may be petrogenetically related to the Ca, Al-rich minerals in Wark-Lovering rims on type A CAIs. AOAs are chondrite components that condensed during the final stage of Wark-Lovering rim formation but, in general, were temporally, spatially, or kinetically isolated from reacting with the nebula vapor during condensation of the lower temperature minerals that were commonly present as chondrule precursors.

---

### INTRODUCTION

Amoeboid olivine aggregates (AOAs) are irregularly shaped, fine-grained aggregates of olivine and, in many cases, contain anorthite, and/or Ca-pyroxene, and/or FeNi metal, and less commonly spinel, perovskite, and melilite. AOAs in CV chondrites have been described by Grossman and Steele (1976), Bar-Matthews et al. (1979), Kornacki et al. (1983), Kornacki and Wood (1984), Hashimoto and Grossman (1987) and Komatsu et al. (2001); in CM chondrites by Cohen et al. (1983), Kornacki et al. (1983); in CO chondrites by Rubin (1985) and Chizmadia et al. (2002); and in CR chondrites by Weisberg et al. (1993) and Aléon et al. (2002). They are minor (less than 1 vol%) components of many carbonaceous chondrites, but some CV chondrites contain up to 9 vol% (McSween 1977a), and some CO chondrites have up to 16 vol% (McSween 1977b). The AOAs in CV chondrites

have been interpreted to be primary nebular condensates (Grossman and Steele 1976), and if they are, AOAs may provide important constraints on models for nebular condensation. AOAs are intermediate in composition and may be a link between the older, refractory calcium-aluminum-rich inclusions (CAIs) and the younger, moderately volatile ferromagnesian chondrules. They may, therefore, provide a genetic link between these objects (e.g., Krot et al. 2002). Additionally, AOAs may be surviving representatives of the precursor solid materials that accreted and were melted to form chondrules (e.g., Grossman and Wasson 1982; Yurimoto and Wasson 2002).

The AOAs in the CR chondrites have a number of intriguing characteristics that prompted this investigation. One of these characteristics is the occurrence of Mn-rich forsterite, in which Fe and Mn are decoupled and Fe/Mn ratios are less than one (Weisberg and Prinz 1990; Weisberg et

al. 1993). Mn-rich olivine that is compositionally similar to that in the AOAs has been found in interplanetary dust particles (IDPs) and as isolated grains in ordinary and carbonaceous chondrite matrices (Klöck et al. 1990). In this paper, we report on the occurrence of Mn-rich forsterite in AOAs and explore its origin and relationship to the more common Mn-poor forsterite in the CR AOAs and chondrules and to Mn-rich olivine in other solar system materials. Olivine in the CR AOAs is  $^{16}\text{O}$ -rich, similar to refractory minerals in CAIs (Aléon et al. 2002), indicating their derivation from an  $^{16}\text{O}$ -rich nebular gas (Krot et al. 2002) and suggesting a primitive origin for the olivine. The AOAs in CR chondrites have not suffered secondary alteration and appear to be pristine examples of early-formed olivine-rich, unmelted refractory inclusions. Some of the AOAs in CR chondrites contain FeNi metal (Weisberg et al. 2002), and in this paper, we explore the texture, composition, and origin of the AOA metal and its relationship to metal in the chondrules in CR chondrites.

Here, we present the results of our study of AOAs in the CR chondrites. We report on the petrology of the olivine, FeNi metal, and other minerals in the AOAs and interpret their petrogenetic histories. Additionally, we report the discovery of an AOA associated with a melilite-rich type A refractory inclusion, allowing us to explore the petrogenetic relationship between AOAs and type A inclusions. Our goals are to present a petrologic report of AOAs in CR chondrites, interpret their origin, and understand their relationship to other chondritic components in the CR chondrites and to AOAs in other chondrite groups.

## METHODS

Eighteen AOAs were located and studied in polished thin sections of eight CR chondrites. The meteorite sections (AOAs) studied included Renazzo AMNH 588-2 (R317, R318), Al Rais AMNH 4168-1 (AR1, AR2), Elephant Moraine (EET) 87770 (EET87-3, EET87-4), EET 92011, 5 (EET920-1, EET920-2), EET 92105, 5 (EET92-12, EET92-21), EET 96259, 6 (EET96-3, EET96-4), El Djouf 001 AMNH 4756-1 (ED1), and Yamato- (Y) 790112 (Y79-1, Y79-2, Y79-3, Y79-4, Y79-5). The inclusions were documented with transmitted light photomicrographs and backscattered electron (BSE) images using the Hitachi S4700 field emission gun scanning electron microscope (FEG-SEM), equipped with a PGT energy dispersive spectrometer (EDS).

Mineral analyses were carried out using a Cameca SX100 electron microprobe. Natural and synthetic standards were chosen based on the compositions of the minerals being analyzed. Silicate compositions were acquired using an accelerating potential of 15 keV and a sample current of 20 nA, and metal compositions were acquired using 20 keV and 25 nA. Counting times were 20 sec on peak and 10 sec on background (off-peak) spectrometer positions. The relative

uncertainties ( $2\sigma$ ), based on counting statistics, for major elements (Si, Fe, Mg) are estimated to be <2%, and for Ti, Cr, Mn and Ca, they are estimated to be 10%, 10%, 9%, and 5%, respectively. The detection limits are 0.05% or less for most elements. Data reductions were carried out using methods described by Pouchou and Pichoir (1991). The Cameca SX100 was also used to collect  $K\alpha$  X-ray maps to study the distribution of minerals in the AOAs.

## RESULTS

### Textures

The AOAs in the CR chondrites are irregularly shaped aggregates of olivine, and in many cases, the olivine occurs in sinuous bands (5–20  $\mu\text{m}$  thick) surrounding nodules of Ca, Al-rich phases and blebs of FeNi metal (Figs. 1a–1e). In general, they lack the spherical (melt-droplet) form and interstitial glassy mesostasis characteristic of many chondrules. Texturally, the AOAs in the CR chondrites are very similar to those in the Allende CV chondrite described by Grossman and Steele (1976) as well as those in CO and CM chondrites. The AOAs in the CR chondrites range in size from about 70  $\mu\text{m}$  to 1.2 mm. Those in CO and CM chondrites are generally <600  $\mu\text{m}$  in size (Rubin et al. 1985), while in CV chondrites, they are generally larger, up to 5 mm in size.

The larger AOAs in the CR thin sections appear to be clusters of numerous nodules (ranging from ~10 to 100  $\mu\text{m}$  in size) consisting of fine olivine or nodules of Ca, Al-rich phases surrounded by sinuous bands of olivine (Figs. 1a, 1b, 1i, and 1j). In thin section, some of the smaller AOAs appear to be fragments of larger aggregates (Fig. 1c), and others appear to be isolated nodules that never accreted into larger aggregates. Individual mineral grains in the AOAs are generally very fine, ranging from <1 to 7  $\mu\text{m}$  in size. The metal blebs in the AOAs have a similar size range from about 0.2 to 7  $\mu\text{m}$ .

The Ca, Al-rich phases in the AOAs include Ti-, Al-rich Ca-pyroxene, anorthite, and, in some cases, spinel and perovskite (Figs. 1a and 1b). In many AOAs, spinel and perovskite occur as sub- $\mu\text{m}$  phases surrounded by anorthite or Ca-pyroxene. However, EET96-1 contains a large nodule composed mostly of spinel (Fig. 1e), and one of the many nodules in R317 contains spinel that is several  $\mu\text{m}$  in size (Fig. 1b). In some AOAs, the Ca-pyroxene appears to be an overgrowth on the olivine or occurs as chains of crystals between the olivine and anorthite (Figs. 1c, 1d, and 1g). Many of the AOAs in CR chondrites contain tiny blebs of FeNi metal (Figs. 1e, 1g, and 1h).

When present, perovskite is surrounded by spinel, and the spinel is surrounded by anorthite, followed by Ca-pyroxene, followed by olivine. Metal generally occurs as blebs surrounded by olivine and, in some cases, occurs within the anorthite in the interior of the refractory nodules. The concentric layering suggests a crystallization sequence of perovskite, spinel, metal,

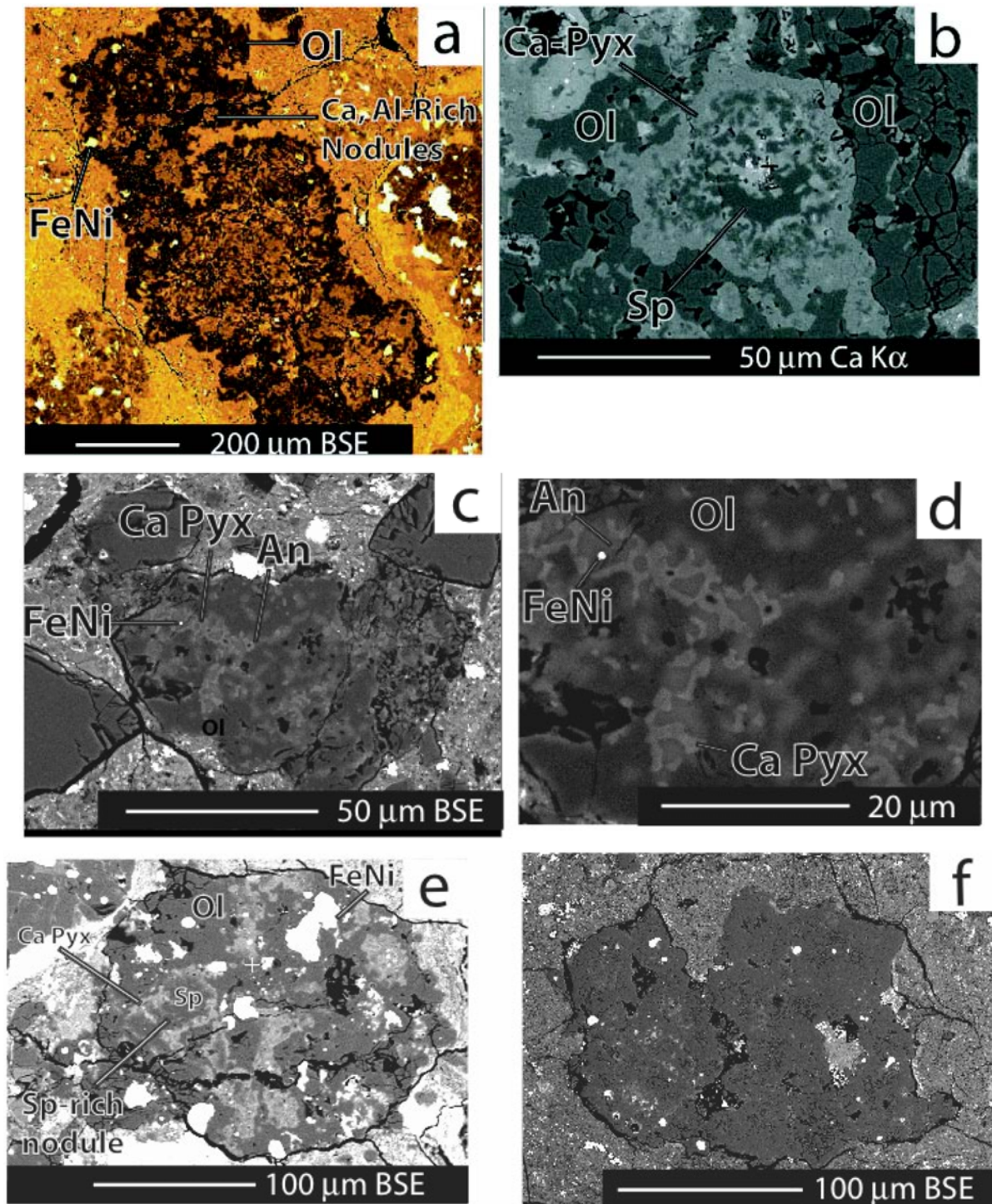


Fig. 1. Backscattered electron (BSE) images and X-ray maps of AOAs in CR chondrites: a) R317 from Renazzo is a relatively large (>600  $\mu\text{m}$  in length) AOA and contains FeNi metal (white) and numerous nodules of Ca-Al-rich assemblages surrounded by sinuous bands of olivine (Ol); b) enlargement of R317 showing a spinel-bearing nodules with spinel (Sp) surrounded by Ca-pyroxene (Ca-Pyx), followed by olivine (Ol); c) EET87-3 from the EET 87770 CR chondrite, consisting of sinuous bands of olivine (Ol) surrounding Ca-pyroxene (Ca-Pyx) and anorthite (An); d) enlargement of a portion of EET87-3 (from [c]) showing the anorthite (An), metal (FeNi metal), and the Ca-pyroxene (Ca-Pyx), which occur as chains of (2  $\mu\text{m}$  size) crystals growing at the boundary between the olivine (Ol) and anorthite; e) EET96-1 is an AOA from EET 96259 that appears to be relatively metal-rich and contains a spinel (Sp)-rich nodule in which spinel is surrounded by anorthite and rimmed by olivine. Other nodules in this inclusion are composed mostly of Ca-pyroxene and anorthite; f) AR-1 from Al Rais is an AOA that contains metal and has a relatively lower abundance of Ca-Al-rich minerals.

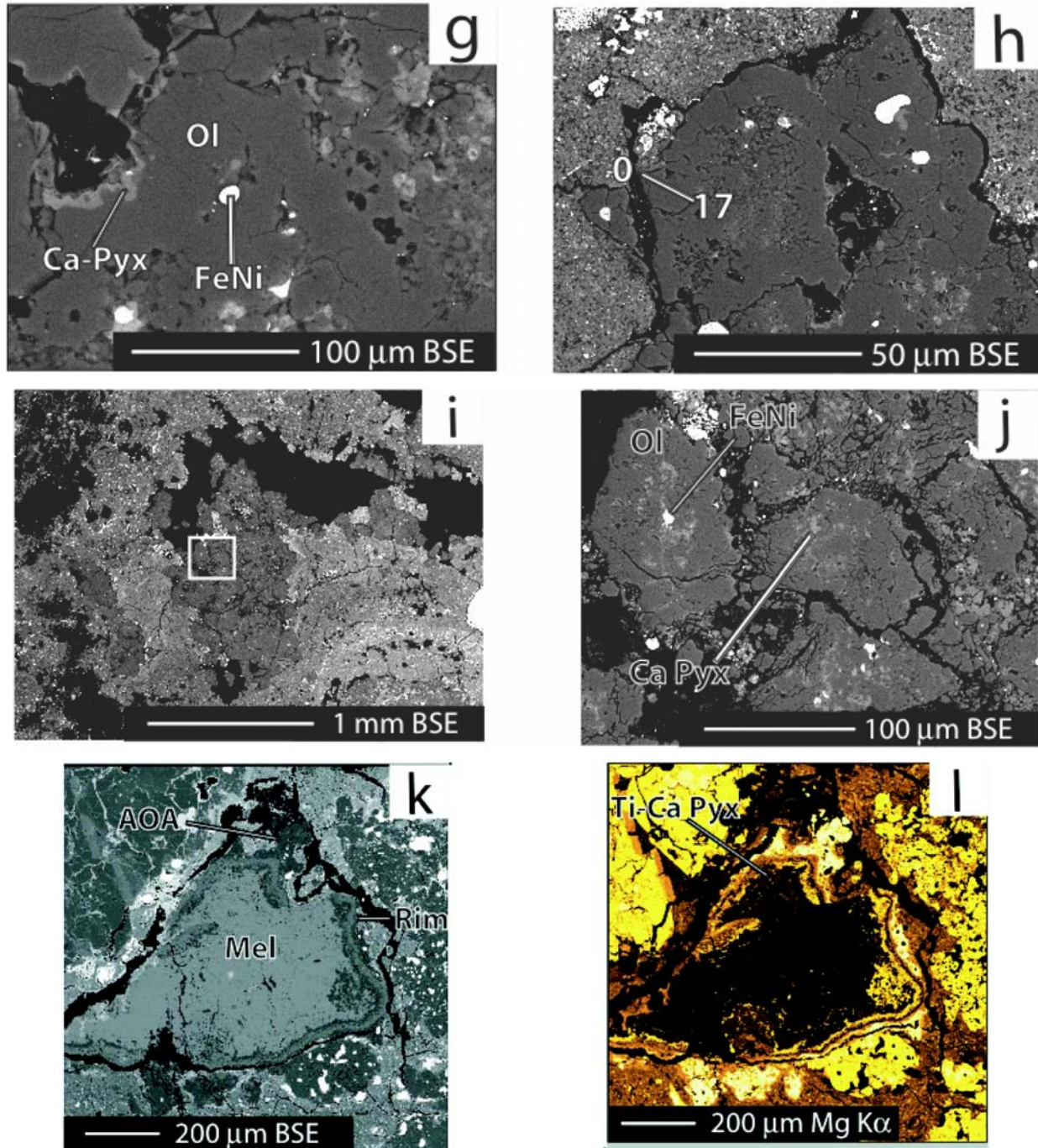


Fig. 1. *Continued.* Backscattered electron (BSE) images and X-ray maps of AOs in CR chondrites: g) enlargement of AR-1 showing a FeNi metal bleb, porosity, and Ca-pyroxene (Ca-pyx) on the surface of the olivine; h) another image of AR-1 showing the sinuous olivine band surrounding a fluffy (porous) region with Ca-Al-rich minerals. The region numbered “0–17” corresponds to electron probe zoning profiles taken along this 17  $\mu\text{m}$ -wide portion of the sinuous olivine band. The compositional profile is displayed in Fig. 3 and shows that the olivine becomes enriched in Mn toward the periphery of the inclusion (point 0); i) AR-2 is a very large (>1.2 mm in length) AO in Al Rais consisting of numerous smaller AOs. This inclusion contains much less Ca-Al-rich minerals than other large inclusions like R317 (shown in [a] and [b]); j) the enlargement shows two of the smaller aggregates that constitute AR-2. They are composed of olivine surrounding small FeNi metal blebs and Ca-pyroxene grains; k) BSE of EET92-21, a compact type A with a coarse (blocky) melilite-rich core surrounded by a Wark-Lovering rim. The outer part of the rim is decorated with AOs; l) Mg K $\alpha$  X-ray map of EET92-21 showing the distribution of AOs (brightest areas) around the edge of the inclusion. The AOs appear very bright because the Mg content of their olivine is greater than that in any of the other olivine in the chondrules or matrix of the meteorite. Ti, Al-rich Ca-pyroxene (Ti-Ca Pyx) is present mainly between the melilite-rich core and the Wark-Lovering rim.

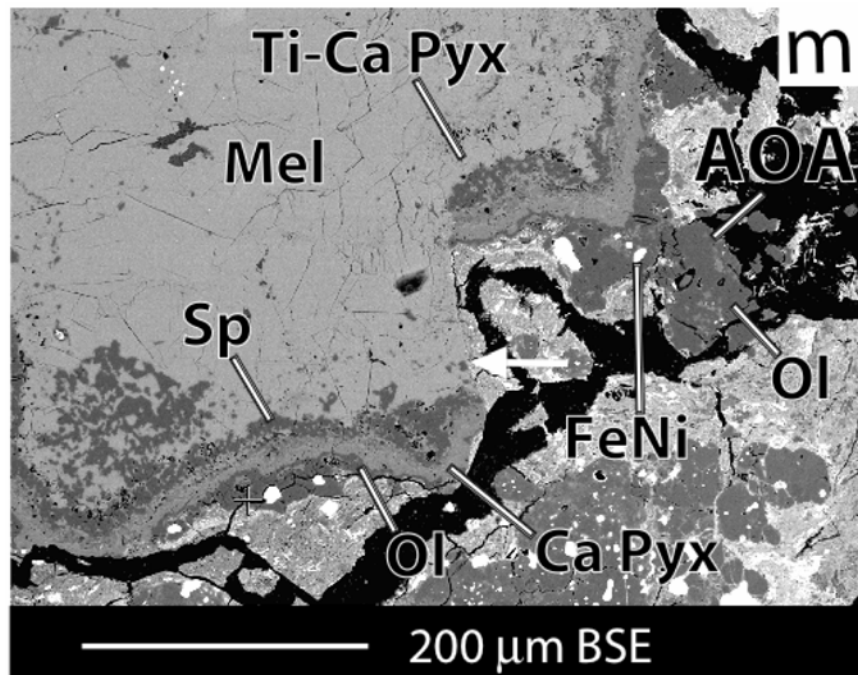


Fig. 1. *Continued.* Backscattered electron (BSE) images and X-ray maps of AOAs in CR chondrites: m) enlargement of the edge of EET92-21 showing the Wark-Lovering rim one of the AOAs on the rim. The AOA contains olivine surrounding Ca-pyroxene and FeNi metal. The Wark-Lovering rim is dislocated along on portion (arrow).

anorthite, Ca-pyroxene, olivine. However, in some cases, the Ca-pyroxene may form from partial melting of the olivine and anorthite assemblage (Komatsu et al. 2002).

The abundances of Ca, Al-rich minerals vary from one AOA to another. R317, for example, has numerous nodules that are rich in Ca-pyroxene (Figs. 1a and 1b). AR1, on the other hand, has only fine regions with Ca-rich phases, primarily diopside occurring along the edges of the olivine (Figs. 1f–1h). AR2 is the largest AOA found in this study, and it contains only minor amounts of Ca, Al-rich minerals. The abundance of metal also varies among the AOAs in CR chondrites. For example, EET96-1 (Fig. 1e) appears to have a higher abundance of metal than other AOAs. However, actual modal mineral abundances are difficult to obtain from thin section of non-symmetric objects, as shown from studies of the three-dimensional petrography of chondrules in CR chondrites (Weisberg et al. 2002; Hertz et al. 2003). The abundances of Ca-Al-rich minerals vary widely among the nodules within a single AOA. EET87-3, for example, contains a spinel-rich nodule, and the other nodules in this AOA are Ca-pyroxene-anorthite assemblages (Fig. 1e).

### Mineral Compositions

Most of the olivine in the AOAs in CR chondrites is near-pure forsterite. However, four of the eighteen AOAs studied contain two different types of forsterite. One type has blue cathodoluminescence (CL) and the other red. The red olivine is much less abundant, and when present, it appears to occur

on the edges of the blue forsterite (Fig. 1h). The CL characteristics of olivine are a result of its low Fe content and trace element composition. Compositionally, the blue forsterite characteristic of most AOAs is minor element-poor having (in wt%)  $<0.05$  MnO and  $<0.15$  Cr<sub>2</sub>O<sub>3</sub>. The red olivine has up to 0.5 Cr<sub>2</sub>O<sub>3</sub> and up to 0.7 MnO (Table 1; Fig. 2a). In some cases, the MnO content of the red olivine equals or exceeds the FeO content. The red forsterites have compositions that are similar to LIME (low-iron Mn-enriched) olivine that has been described in interplanetary dust particles (IDPs), as well as isolated Mn-rich forsterite grains in the opaque matrices of the Murchison (CM2) and Semarkona (LL3) chondrites (Klöck et al. 1989; Figs. 2 and 3).

The olivine in the AOAs differs dramatically in composition from olivine in type I chondrules in the CR chondrites. The Fe content of the AOA olivine is generally much lower than that in the olivine of type I chondrules. In type I olivine, Fe and Mn are positively correlated, and the Mn/Fe ratios are never greater than or even close to one (Fig. 2). The Mn-enrichment of the olivine in the CR AOAs generally occurs at the edges of the inclusion and shows no correlation with the Fe content of the olivine (Fig. 3).

Ca-pyroxene contains (in wt%) up to 1.6 TiO<sub>2</sub> and 6 Al<sub>2</sub>O<sub>3</sub> and is similar in composition to the pyroxene in AOAs in the Allende CV chondrite (Grossman and Steele 1976). REEs were measured in the Ca-pyroxene from the AOA in Renazzo shown in Fig. 1a. Its pattern is essentially flat but exhibits a slight enrichment in the heavy REEs. La is

Table 1. Representative analyses (wt%) of olivine in AOAs in CR chondrites.<sup>a</sup>

	E87-5	E87-3	Y79-3	Y79-3	R317	AR-1	AR-2
SiO <sub>2</sub>	42.6	42.7	42.2	42.3	42.4	42.8	42.8
CrO	bd	0.29	0.12	0.26	0.17	0.29	0.21
FeO	0.37	0.43	0.48	0.52	0.35	0.23	0.29
MnO	bd	0.52	bd	0.33	bd	0.38	bd
MgO	56.5	56.2	56.0	56.3	56.3	56.4	56.4
CaO	0.37	0.05	0.12	0.10	0.16	0.03	0.05
Total	99.84	100.20	98.92	99.81	100.15	100.13	99.75
Fa (mol%)	0.4	0.4	0.5	0.5	0.4	0.2	0.3

<sup>a</sup>bd = below detection (<0.05%); TiO<sub>2</sub> and Al<sub>2</sub>O<sub>3</sub> are below detection for all analyses.

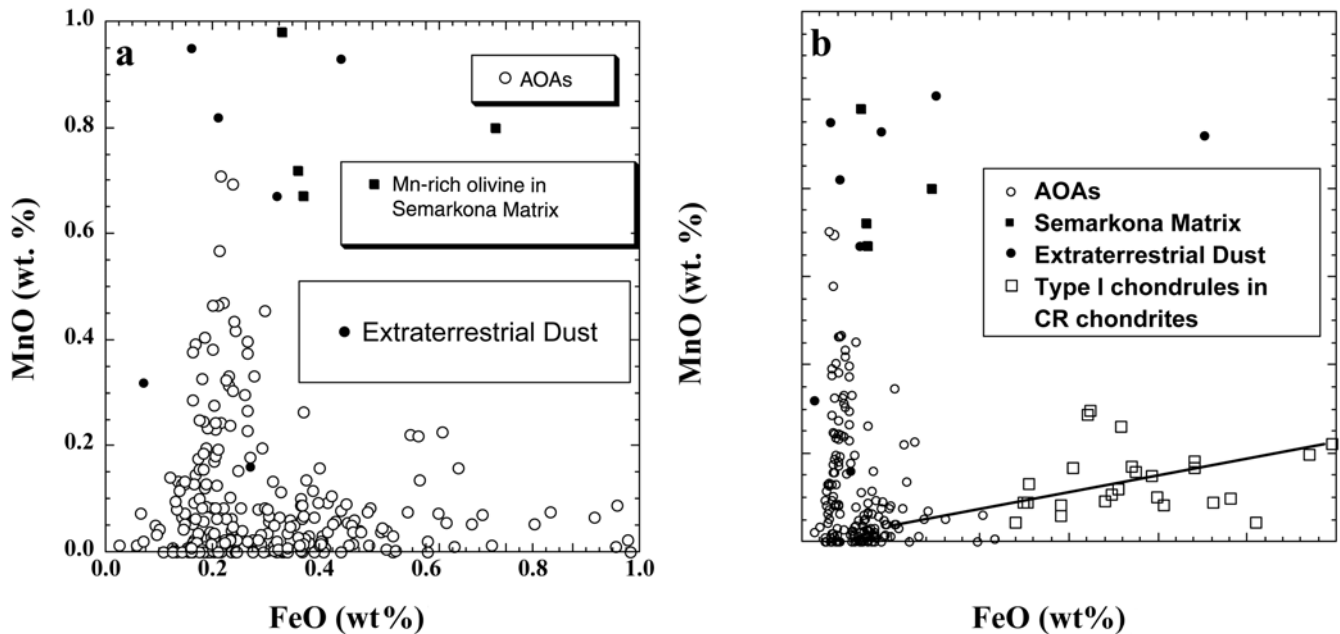


Fig. 2. a) Plot of FeO versus MnO for olivine in AOAs in the CR chondrites. Some of the olivine in the AOAs have high Mn contents, and in some cases, the Mn content is equal to or higher than the Fe content. Also shown on this diagram are Mn-rich olivine (called “LIME”) from the interplanetary dust particles (IDPs) and in the matrix of the Semarkona LL3.0 chondrite; b) plot of FeO versus MnO showing compositions of olivine in the AOAs compared with those in type I chondrules in CR chondrites. Chondrule olivine differs from that in the AOAs in having higher FeO, a MnO content that never equals or exceeds the FeO content, and a general positive relationship between the FeO and MnO contents.

~15–25× chondritic and Lu is 28–40× chondritic, with a small negative Eu anomaly, most pronounced in one pyroxene (Weisberg et al. 1991). Whole AOAs in CV chondrites were shown to have essentially flat REE patterns and some have fractionated patterns that are similar to the group II patterns of fine-grained CAIs (Grossman et al. 1979).

Plagioclase in the AOAs is near-pure anorthite with Na and K below microprobe detection limits (~0.05). Spinel and perovskite, when present, are generally too fine (less than ~2 μm) to analyze by EPMA. The spinel is commonly near-pure MgAl<sub>2</sub>O<sub>4</sub> by EDS analysis. In some cases, it contains tiny perovskite inclusions, and the spinel is surrounded by anorthite and Ca-pyroxene. One inclusion (EET87-3) contains a large aggregate of spinel surrounded by anorthite (Fig. 1e).

Metal blebs in the AOAs are compositionally similar to metal in chondrules and matrix in the CR chondrites. They

have 5 to 7.2 wt% Ni and an approximately solar Ni:Co ratio, similar to metal in the type I chondrules in CR chondrites (Fig. 4). In CR chondrite chondrules, metal occurs as rounded blebs within the chondrule cores and as smaller blebs in rims surrounding the chondrules (Weisberg et al. 1993; Hertz et al. 2003). The metal in the chondrule cores generally has higher Ni than that in the rims (Weisberg et al. 1990, 1993). The Ni and Co content of the metal in the AOAs in CR chondrites overlaps with that of metal in the chondrule rims and some chondrule cores.

#### EET92-21 and Timing of AOA and CAI Formation

EET92-21 is described separately here because it reveals an important textural relationship. It is a typical compact type A inclusion with AOAs occurring adjacent to its Wark-

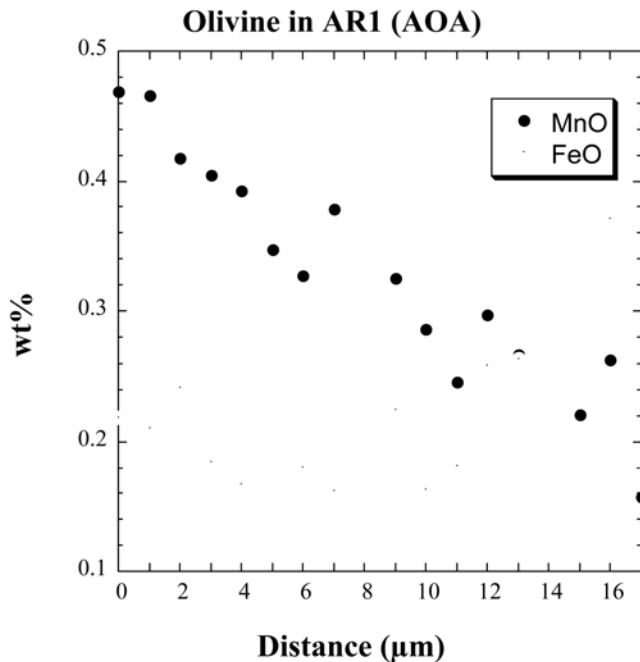


Fig. 3. Compositional (wt% MnO and FeO) zoning profile taken from the outer edge (0  $\mu\text{m}$ ) to the inner edge (17  $\mu\text{m}$ ) of the sinuous olivine band in an AOA (AR-2) from Al Rais (see Fig. 1h). This AOA has Mn-rich olivine at its edge, and the zoning profile shows an increase in MnO from about 0.15 in the inner edge of the band to 0.47 at the outer edge of the band. FeO shows no increase, and the measured MnO:FeO ratio is about 2 at the edge of the band. The true MnO contents of the edge may be higher, but the analyses are limited by the 2  $\mu\text{m}$  spatial resolution of the electron probe beam.

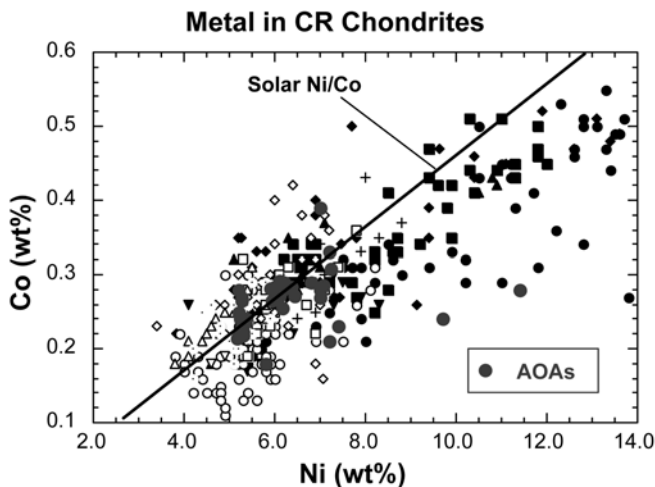


Fig. 4. Plot of Ni versus Co (wt%) showing compositions of FeNi metal in the AOAs in CR chondrites. Also shown is metal from the rims and cores of chondrules in the CR chondrites. Like metal in the chondrules, the AOA metal has positive Ni-Co relationship with Ni:Co ratios that are close to the solar ratio. The AOA metal has compositions that are similar to rim metal and some core metal in the chondrules.

Lovering rim (Figs. 1k, 1l, and 1m). Its core consists mainly of coarse blocky melilite with MgAl spinel and perovskite. Surrounding the inclusion is a Wark-Lovering rim containing, in sequence from the inner to the outer edge—spinel, melilite, cpx-spinel—with olivine present in some portions of the rim (Fig. 1l). The olivine in the rim appears to be near-pure forsterite similar to that in the AOAs (Table 3). The whole type A inclusion is broken along one edge, and the rim is not present along this portion.

In addition to olivine occurring as part of the rim of this type A inclusion, AOAs are attached to the rim in three locations (Figs. 1k, 1l, and 1m). The AOAs consist of olivine with anorthite and Ca-Pyx and FeNi metal, texturally and compositionally similar to the other AOAs described above (Table 3). In one location, the Wark-Lovering rim is displaced, suggestive of fracturing and faulting of the inclusion after formation of the rim (Fig. 1m). However, the fracture, along which the displacement occurred, is not visible within the inclusion, indicating that it was healed during or before recrystallization of the melilite core. A portion of the Wark-Lovering rim appears to have been dislodged and is included within the interior of the CAI (Fig. 1k). Based on these observations, this final stage of fracturing and recrystallization occurred after the condensation of olivine, which forms a layer in the Wark-Lovering rim.

## DISCUSSION

### Primitive Origin of the AOAs

The AOAs in CV chondrites have been interpreted to be aggregates of solid nebular condensates (e.g., Grossman and Steele 1976) and the AOAs in the CR chondrites have similar characteristics that suggest they too did not crystallize from liquids (Aléon et al. 2002). AOAs have highly irregular shapes that differ from the spherical to semi-spherical once-molten chondrules. They do not appear to contain glassy mesostasis like that found in many chondrules, and they contain porosity suggesting they formed from aggregation of solids. They appear to be aggregates of nodules, with some nodules having a concentric layered mineralogy of perovskite and spinel surrounded by anorthite surrounded by Ca-pyroxene, followed by olivine. The diversity of nodules within a single AOA (e.g., EET87-3, as shown in Fig. 1e) also attests to the aggregational, unmelted character of the AOAs. Aléon et al. (2002) showed that the olivine in AOAs in CR chondrites is  $^{16}\text{O}$ -rich, similar to unmelted CAIs, while in igneous CAIs, some minerals are  $^{16}\text{O}$ -rich because they experience isotopic exchange with the  $^{16}\text{O}$ -poor reservoir during melting. These findings suggest that AOAs in CR chondrites are more primitive than melted CAIs.

We suggest that the AOAs in CR chondrites had a complex petrogenetic history that included nebular gas-solid condensation, partial reaction of mineral phases with the

Table 2. Representative analyses (wt%) of refractory phases in AOAs in CR chondrites.<sup>a</sup>

	R317		EET87-3		Y79-1	
	Spinel	Ca-Pyx	Ca-Pyx	Spinel	Ca-Pyx	Spinel
SiO <sub>2</sub>	0.19	48.6	52.3	0.15	50.3	4.3
TiO <sub>2</sub>	0.6	1.3	0.3	0.8	0.7	1.2
Al <sub>2</sub> O <sub>3</sub>	70.6	6.5	3.0	70.8	1.4	63.4
Cr <sub>2</sub> O <sub>3</sub>	0.6	bd	bd	0.13	0.11	0.9
FeO	0.1	0.4	0.6	0.3	0.3	0.6
MnO	bd	bd	bd	0.07	bd	bd
MgO	27.3	16.5	18.4	27.3	25.2	26.6
CaO	0.2	24.9	24.3	0.11	20.9	2.6
Total	99.59	98.20	98.90	99.66	98.91	99.60

<sup>a</sup>bd = below detection (<0.05%); vanadium in spinel is below detection; SiO<sub>2</sub> and CaO in the spinel are presumably due to overlap with adjacent silicate.

Table 3. Representative analyses (wt%) of minerals in the EET92-21 type A inclusion core, Wark-Lovering rim, and the AOA attached to the rim.<sup>a</sup>

	Core melilite	Core melilite	Core Ti, Ca-Pyx	Rim spinel	Rim melilite	Rim anorthite	Rim Ca-Pyx	Rim olivine	AOA olivine	AOA Ca-Pyx	AOA anorthite
SiO <sub>2</sub>	24.7	27.5	32.1	0.3	25.7	41.1	52.2	43.2	42.9	53.8	41.6
TiO <sub>2</sub>	bd	bd	13.6	0.2	0.1	bd	0.5	bd	bd	bd	bd
Al <sub>2</sub> O <sub>3</sub>	31.0	26.8	22.5	71.3	30.0	34.3	3.8	0.2	bd	0.9	36.8
Cr <sub>2</sub> O <sub>3</sub>	bd	bd	bd	0.3	bd	bd	bd	0.1	0.1	bd	bd
FeO	bd	bd	bd	bd	bd	bd	0.3	1.0	0.7	0.4	0.1
MnO	bd	bd	bd	bd	bd	bd	bd	bd	bd	bd	bd
MgO	2.0	3.6	6.4	28.0	2.7	0.3	21.0	54.9	56.8	18.2	1.4
CaO	41.2	41.1	24.9	0.2	40.8	23.5	23.1	0.5	0.1	24.8	19.5
Total	98.9	99.0	99.5	100.3	99.3	99.2	100.9	99.9	100.6	98.1	99.4

<sup>a</sup>bd = below detection (<0.05%); core melilite analyses were selected to illustrate the range of compositions in the melilite; core Ti, Ca-Pyx occurs at the interface between the core and the Wark-Lovering rim; see Figs. 11 and 1m.

cooling nebular gas, accompanied by sintering and coarsening of the assemblage. Based on the concentric sequence of minerals inferred from the thin section, perovskite and spinel are the highest temperature condensing phases preserved in the AOAs. Figure 5 presents the predicted sequence of phases condensing in thermodynamic equilibrium with a solar gas at total pressures ( $P^{\text{tot}}$ ) of  $10^{-3}$  and  $10^{-5}$  bar, based on the work of Ebel and Grossman (2000). Perovskite begins to condense at temperatures ( $T$ ) as high as 1680 and 1530, at  $P^{\text{tot}}$  of  $10^{-3}$  and  $10^{-5}$  bar, respectively (Fig. 5). Spinel condenses about 200° lower, however, melilite condenses at  $T$  halfway between perovskite and spinel (e.g., at 1580 K at  $10^{-3}$  bar) and reacts with perovskite and vapor to form spinel and Ti-, Al-rich Ca-pyroxene (cpx) above the  $T$  where olivine appears (cf. Grossman 1972; Yoneda and Grossman 1995). After olivine becomes stable, feldspar (nearly pure anorthite) forms through the reaction of spinel and cpx with vapor, or through the reaction of melilite with vapor at lower  $P^{\text{tot}}$  (e.g.,  $10^{-8}$  bar). Feldspar condenses before olivine only at or below  $P^{\text{tot}} \sim 10^{-8}$  bar, but at  $10^{-8}$  bar, metal condenses after olivine and orthopyroxene. The presence of metal suggests the assemblage formed at a relatively high  $P^{\text{tot}}$ , and with the exception of anorthite, the observed assemblage is more consistent with the condensation sequence predicted at  $10^{-3}$  bar. The experimental constraints on thermodynamic models

for Ca-rich, Ti-, Al-bearing pyroxene solid solutions are very weak (Sack and Ghiorso 1994), and the models are difficult to implement in condensation calculations. Although pyroxene affects condensation of feldspar and olivine, it is unlikely that the cpx models used here and elsewhere (e.g., Yoneda and Grossman [1995], following Beckett [1986]) are wrong in such a way that the olivine-feldspar prediction is wrong. The mineral sequence—perovskite, spinel, metal, anorthite, and/or cpx-olivine—cannot be achieved directly through equilibrium condensation during cooling of a gas of solar composition at any reasonable nebular pressure.

The AOAs preserve some fraction of condensed perovskite and spinel that was not available to react with vapor at lower  $T$ . The aggregates remained hot long enough for their grains to sinter and coarsen, but concentric layering of these minerals indicates some degree of disequilibrium in the system. Anorthite appears at a textural location perhaps formerly occupied by melilite. Before and during olivine condensation, nebula vapor would have been rich in SiO. Anorthitic feldspar may result from the reaction of previously formed melilite with SiO after the onset of olivine condensation. Alternatively, metastable anorthite may have formed from pre-existing melilite in a reaction relation with cpx and spinel (i.e., less energy is required to form anorthite by adding SiO to melilite than to form cpx reconstructively from melilite). These scenarios are consistent with the

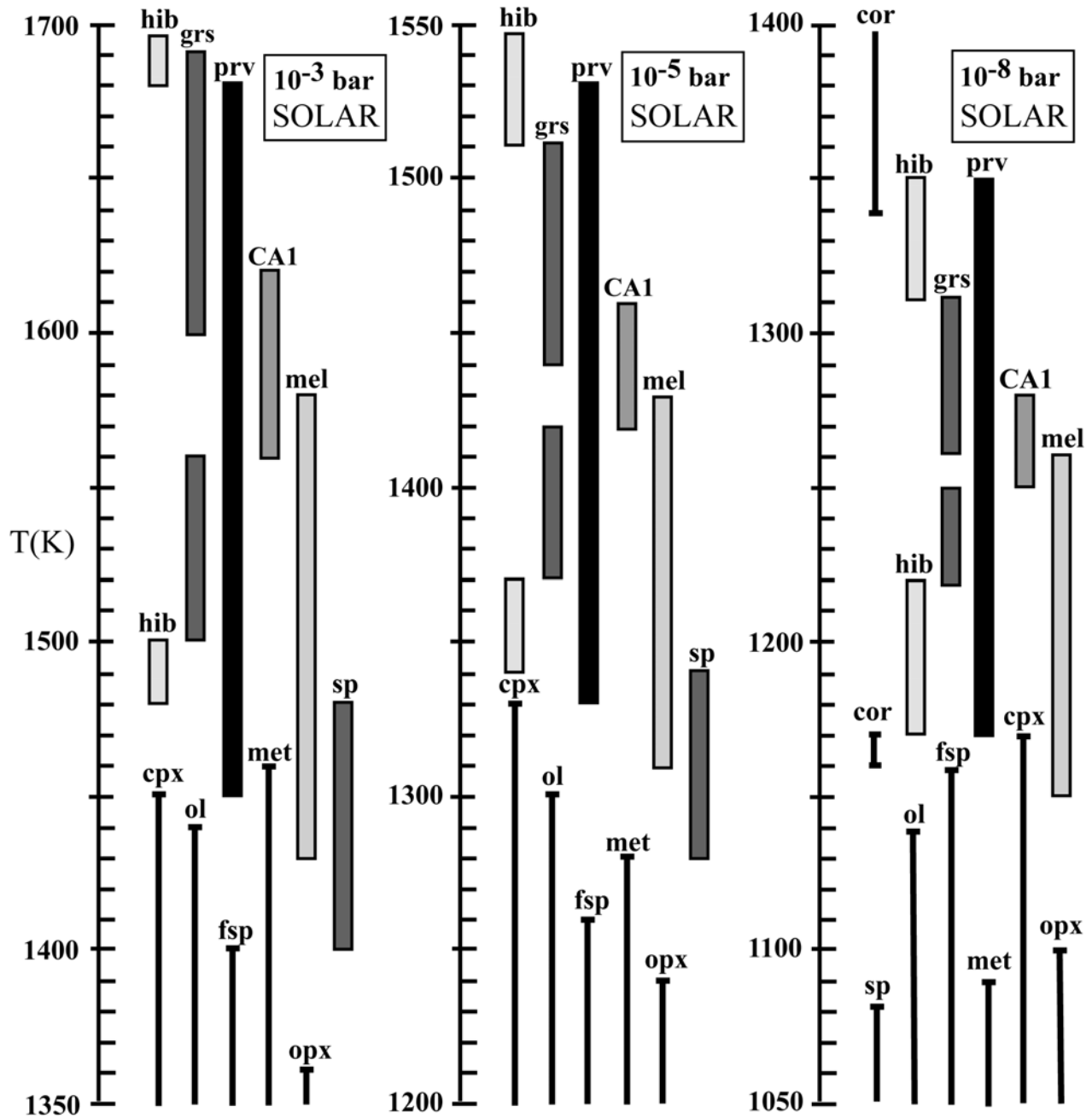


Fig. 5. Appearance and disappearance temperatures of phases hibonite/grossite/Ca-aluminate ( $\text{CaAl}_2\text{O}_4$ )/melilite/spinel/metal. Phase appearances/disappearances, as in Ebel and Grossman (2000), agree very closely with Yoneda and Grossman and Grossman (1972), below the appearance temperature of spinel, which is the region of interest here. The same thermodynamic models were used as those described in Ebel and Grossman (2000); hib = hibonite, grs = grossite, prv = perovskite, CA1 =  $\text{CaAl}_2\text{O}_4$ , mel = melilite, cpx = Ca-pyroxene, met = Fe, Ni metal, ol = olivine, fsp = feldspar, sp = spinel, opx = low-Ca pyroxene.

observed mineral sequence. If for some kinetic reason cpx failed to nucleate, as predicted by equilibrium models, then late stage cpx might be the result of later reheating and minor melting of anorthite and olivine, as demonstrated by Komatsu et al. (2002).

We did not find low-Ca pyroxene associated with the AOAs that we studied. However, Krot et al. (2003) found that

10% of the AOAs in the CR chondrites they studied contain low-Ca pyroxene grains on their edges beyond olivine. They suggested that the low-Ca pyroxene formed by reaction of olivine with the nebular gas reservoir. This is consistent with our condensation prediction at all pressures (Fig. 5). AOAs that lack low Ca-pyroxene were either spatially isolated from the nebula or kinetically inhibited from reacting with nebular

vapor at temperatures above 1360 K, where low-Ca pyroxene is stable at  $P^{\text{tot}} = 10^{-3}$  bar (Fig. 5).

### Formation of Mn-Rich Forsterite

Similarities in the cosmochemical behaviors of Fe and Mn usually result in co-variation of these elements during igneous fractionation. Melting of chondritic starting materials results in a general coupling of Fe and Mn as observed in the type I chondrules in CR chondrites (Fig. 2). However, in the AOAs, Fe and Mn are decoupled, as shown in Figs. 2 and 3, and formation of Mn-rich forsterite requires a mechanism that decouples these elements. Two mechanisms for formation of the Mn-rich forsterite in AOAs are considered here: 1) direct nebular condensation, and 2) reduction of Fe in the olivine.

Klöck et al. (1989) offered a condensation scenario for the “LIME” olivine in IDPs and chondrite matrices, and the Mn-rich forsterite in the AOAs may have formed in a similar manner. When present in the CR AOAs, Mn-rich forsterite generally surrounds pure forsterite. Thus, formation of Mn-rich forsterite later than the pure forsterite is a required prediction of any model for their origin. Pure forsterite is stable in a solar gas below ~1440 K (at  $10^{-3}$  atm) according to our thermodynamic modeling of the order of condensing phases (Fig. 5), which is consistent with earlier thermodynamic simulations (e.g., Larimer 1967; Grossman 1972; Ebel and Grossman 2000). Pure forsterite may have nucleated or aggregated onto the surfaces of earlier-formed (1600–1440 K) phases in the Ca-Al-rich nodules. These aggregates later equilibrated with the nebula down to about 1100 K, the temperature at which  $\text{Mn}_2\text{SiO}_4$ , the tephroite molecule, is predicted to form in solid solution with forsterite (Wai and Wasson 1977). Fayalitic olivine becomes stable in a gas of solar composition at much lower temperatures (~500 K) via a reaction of Fe-metal with forsteritic olivine with vapor. The high Mn/Fe ratio of the Mn-rich forsterite suggests that the forsterite did not equilibrate with Fe-metal at much lower nebular temperatures, and the surrounding vapor did not have a high  $f\text{O}_2$  or enrichment in dust (Ebel and Grossman 2000). The Mn-rich forsterite rims on some AOAs may represent olivine grains that aggregated onto the outer surface of AOAs or that are the result of partial equilibration of the outer portions of existing aggregates with the surrounding nebular gas in a cooling system. One problem with this scenario is the absence of low-Ca pyroxene, which condenses at about 1360 K. However, Imae et al. (1993) experimentally addressed the formation of enstatite in the nebula via a reaction of forsterite and Si-rich residual nebular gas. They showed that the rate of reaction is fairly slow and very little enstatite would form in a cooling nebula.

Reduction of iron from olivine could also yield olivine with a high Mn/Fe ratio. In this scenario, the Mn-rich forsterite may have lost Fe through reduction reactions between the olivine and the surrounding nebular gas or the

surrounding matrix on the parent body. The FeNi metal in the AOAs could be a product of such a reduction reaction. Lee et al. (1992) found that some metal in the Renazzo CR chondrite is zoned with Ni and Co decreasing and Fe increasing at the edges of the grains. They interpreted the low Ni and Co to be the result of dilution by Fe, produced by a FeO reduction during metamorphism on the CR parent body. The occurrence of Mn-rich forsterite on the edges of the AOAs is consistent with this interpretation. However, there is no other evidence for reduction in the AOAs. If the Mn-rich forsterite formed by reduction of Fe from silicate, a relationship between the relative abundances of Mn-rich forsterite and metal in the AOAs might be expected, and no such relationship is apparent. The reduction of Fe in olivine would also result in the formation of silica or low-Ca pyroxene and these minerals are not found in the AOAs that we studied. Additionally, the AOAs are interpreted to be high temperature condensates, and substantial Fe is not expected to be present in the olivine.

There is clear evidence that the Mn-rich forsterite did not form on the parent body. If parent body reduction were responsible for formation of the Mn-rich forsterite, one might expect a fairly uniform distribution of Mn-rich olivine around the edge of any particular AOA, and all AOAs from a single meteorite might be expected to contain Mn-rich olivine. This is not the case. In AR1, some edges have Mn-rich forsterite, while others do not, and AR2, which is located in the same thin section as AR1, does not contain Mn-rich forsterite. The presence of Mn-rich forsterite in the least equilibrated chondrites (including Murchison and Semarkona) in IDPs (Klöck et al. 1970), and now the CR chondrites is inconsistent with formation of Mn-rich forsterite by parent body metamorphism and favors formation of the Mn-rich olivine by solid-gas reactions in the nebula.

### Origin of Metal in the AOAs

The AOAs in the CR chondrites contain blebs of FeNi metal within and surrounded by olivine. Metal blebs also occur within the Ca-Al-rich nodules in AOAs. The shape and composition of the metal is similar to that in the type I chondrules in the CR chondrites (Weisberg et al. 1993), and may have a similar origin. However, the AOAs in the CR chondrites that contain metal appear to be irregularly shaped aggregates that have not been extensively melted (e.g., Fig. 1), as argued above.

The origin of metal in chondrules and matrix in the CR chondrites has been a controversial issue. Metal was shown to have a solar Ni:Co ratio consistent with an origin as a primary condensate (Weisberg et al. 1993; Grossman and Olsen 1974). Petrologic studies and trace compositions of some metal in CR chondrules have been interpreted as being inconsistent with a condensation origin (Connolly et al. 2001; Humayun et al. 2002) and have led workers to suggest formation by reduction during chondrule formation, vaporization and

recondensation (e.g., Connolly et al. 2001), or devolatilization of iron sulfides (e.g., Zanda et al. 2002).

Formation of the FeNi metal in the AOA by reduction during melting or solid-state reduction would require that the AOA olivine was initially more FeO-rich than it currently is. From thermodynamic considerations (e.g., Grossman 1972), FeO in olivine is not expected to be associated with high temperature condensates from a gas of solar composition. Therefore, FeO-bearing olivine is not compatible with the Ca-Al-rich, volatile element-poor assemblages in the AOAs. FeO-bearing olivine has been found associated with AOAs in Allende, however, this olivine is interpreted to have formed by secondary metasomatic processes in the nebula or on the parent body (e.g., Krot et al. 1995). Additionally, the high Ni content of the metal (Fig. 4) also suggests that the metal did not form through reduction of Fe. Reduction of Fe from olivine may also be expected to result in the formation of silica or low-Ca pyroxene, which was not found in the AOAs that we studied.

It is possible that some metal in the AOAs formed initially as a direct condensate from a vapor, presumably the solar nebular gas. The metal grains may have acted as nuclei for growth of the olivine. At a pressure of  $10^{-3}$  bar, FeNi metal begins to condense (at 1460 K) before forsterite (1440 K). Metal stability overlaps with melilite in the range of 1460 K to 1430 K at  $10^{-3}$  bar (Fig. 5). This is consistent with the observation of metal surrounded by olivine, as well as within the Ca, Al-rich nodules in AOAs. Trace (platinum group) element analysis of the metal is needed to further test the hypotheses for the origin of the metal in the AOAs.

### Relationship of the AOAs to CAIs and Chondrules

From the textural relationship revealed in EET92-21 (Figs. 1k, 1l, and 1m), the AOAs appear to have crystallized at the end stages of the Wark-Lovering rim formation. This observation documents a clear temporal relationship between type A CAIs and the AOAs in the CR chondrites. Krot et al. (2001, 2002) also showed a relationship between AOAs and forsterite-rich accretionary rims around CAIs. Type A CAIs are generally devoid of olivine in their interiors. On the other hand, the AOA olivine has a lower (mol%) fayalite component than that in chondrule olivine, and the AOAs generally lack low-Ca-pyroxene and the lower temperature (Na- and K-bearing) phases that are generally present in chondrules. Therefore, the AOAs apparently formed between the episode(s) of Wark-Lovering rim formation on CAIs and the bulk of chondrule formation. They represent an intermediate temperature and/or time between formation of the refractory-rich CAIs and the moderately volatile chondrules.

The formation of Wark-Lovering rims is a controversial issue. Wark and Lovering (1977) suggested that the rims around type A and type B Ca, Al-rich inclusions represent a stratigraphic sequence of condensation and aggregation of solids in the nebula before the condensation of olivine.

However, the Wark-Lovering rim sequences may also be vaporization residues (e.g., Boynton and Wark 1985) or the result of repeated cycles of vaporization and recondensation (e.g., Niederer et al. 1985). Murrell and Burnett (1987) reviewed several mechanisms for rim formation including transient heating in a planetary atmosphere, fluctuating temperatures in the nebula, passage of the CAI through different temperature regimes, direct nebular condensation, and vaporization and recondensation. They concluded that all mechanisms remain possible and that each rim layer may have had a separate origin. In the case of the EET92-21 Compact Type A inclusion, we conclude that the formation of AOAs represents the final stages of rim formation. The AOAs in EET92-21 may have condensed onto the Wark-Lovering rim or were available as free-floating objects that accreted onto the inclusion. The layer of olivine in the rim suggests that olivine condensed at the final stages of rim formation.

The type A CAIs, like EET92-21, experienced complex petrogenetic histories that included multiple cycles of heating resulting in the formation of Wark-Lovering rims. Condensation of olivine occurred at the final stages and continued after Wark-Lovering rim formation. Based on EET92-21, the AOAs formed after Wark-Lovering rim formation. The Ca, Al-rich assemblages that are present in the AOAs may have formed by the same or similar event as did Wark-Lovering rims. The lack of more volatile elements in the AOAs suggests that they were spatially, temporally, or kinetically isolated from the nebula at the lower temperatures at which low-Ca-pyroxene- and volatile-bearing chondrule precursor materials condensed. Low-Ca-pyroxene condenses from a gas of solar composition at about 1360 K at  $10^{-3}$  and 1240 K at  $10^{-5}$  bar (Fig. 5).

The rim on EET92-21 is broken and dislocated (Fig. 1m). The fracture along which displacement occurred is healed, and a portion of the rim is included within the recrystallized coarse, melilite-rich interior of the CAI. Thus, this final episode of fracturing and recrystallization (reheating) occurred after the condensation of olivine. This CAI may have experienced multiple excursions into hotter regions of the nebula (e.g., Cassen 2001) or experienced pulses of energy like those produced by shock waves (e.g., Desch and Connolly 2002) or current sheets (e.g., Jung et al. 2004) in the protoplanetary disk.

### CONCLUSIONS

1. The AOAs in CR chondrites have irregular shapes, fluffy textures, and lack the glassy mesostasis found in chondrules, suggesting that they are aggregates, most likely of nebular condensates.
2. Many larger AOAs in CR chondrites are clusters of smaller aggregates.
3. The petrogenetic history of the AOAs in CR chondrites included nebular gas-solid condensation, reaction of

minerals with the nebular gas, small degrees of melting, and sintering of the assemblage. The mineral assemblages of the AOAs are most consistent with nebular condensation modeled at relatively high nebular pressures near  $10^{-3}$  bar.

4. Some AOAs in CR chondrites contain Mn-rich forsterite with Mn/Fe ratios greater than one. These AOAs equilibrated with the surrounding gas down to about 1100 K, the temperature at which the tephroite ( $\text{Mn}_2\text{SiO}_4$ ) molecule condenses in solid solution in forsterite (Wai and Wasson 1977). The Mn-rich forsterite is a component of many primitive solar system materials including IDPs, unequilibrated ordinary chondrite matrix, and AOAs in CR chondrites. The Mn-rich forsterite in all of these primitive materials may have had a similar origin.
5. FeNi metal in the AOAs in CR chondrites is compositionally similar to metal in the CR chondrules, as well as metal in other primitive materials such as Murchison. This metal may have condensed initially as a solid from the nebula gas and acted as nuclei for growth of olivine.
6. The AOAs are an intermediate chondritic component that was in equilibrium with the surrounding gas during or after the final stage of Wark-Lovering rim formation on type A CAIs. But, AOAs were temporally or spatially isolated from or kinetically inhibited from reacting with the nebula vapor during formation of lower temperature condensates, e.g., low-Ca-pyroxene and other more volatile constituents of chondrule precursors.

*Acknowledgments*—The authors wish to thank the American Museum of Natural History and the Meteorite Working Group for supplying meteorite thin sections of CR chondrites. Additionally, Charlie Mandeville (AMNH electron Probe), Angela Klaus, and Kevin Frishman (AMNH scanning electron microscope) are thanked for analytical and technical assistance. The authors also thank reviewers Tim Fagan and Sasha Krot and associate editor Hiroko Nagahara for thoughtful and detailed reviews that led to substantial improvement of the paper. This project was supported by NASA Cosmochemistry Grants NAG5–11546 (M. K. Weisberg, P.I.) and NAG5–12855 (D. S. Ebel, P.I.)

*Editorial Handling*— Dr. Hiroko Nagahara

## REFERENCES

- Aléon J., Krot A. N., and McKeegan K. D. 2002. Calcium-aluminum-rich inclusions and amoeboid olivine aggregates from the CR carbonaceous chondrites. *Meteoritics & Planetary Science* 37:1729–1755.
- Bar-Matthews M., MacPherson G. J., and Grossman L. 1979. An SEM-petrographic study of amoeboid olivine aggregates in Allende. *Meteoritics* 14:342.
- Beckett J. R. 1986. The origin of calcium-aluminum-rich inclusions from carbonaceous chondrites: An experimental study. Ph.D. dissertation, University of Chicago, Chicago, Illinois, USA.
- Boynton W. V. and Wark D. A. 1985. Refractory rims: Evidence for high temperature events in the post formation history of Ca-Al-rich inclusions (abstract). *Meteoritics* 20:613–614.
- Cassen P. 2001. Nebular thermal evolution and the properties of primitive planetary materials. *Meteoritics & Planetary Science* 36:671–700.
- Chizmadia L. J., Rubin A. E., and Wasson J. T. 2002. Mineralogy and petrology of amoeboid olivine inclusions in CO3 chondrites; Relationships to parent body aqueous alteration. *Meteoritics & Planetary Science* 37:1781–1796.
- Cohen R. E., Kornacki A. S., and Wood J. A. 1983. Mineralogy and petrology of chondrules and inclusions in the Mokoia CV3 chondrite. *Geochimica et Cosmochimica Acta* 47:1739–1757.
- Connolly H. C., Huss G. R., and Wasserburg G. J. 2001. On the formation of Fe-Ni metal in Renazzo-like carbonaceous chondrites. *Geochimica et Cosmochimica Acta* 65:4567–4588.
- Desch S. J. and Connolly H. C., Jr. 2002. A model for the thermal processing of particles in solar nebula shocks: Application to the cooling rates of chondrules. *Meteoritics & Planetary Science* 37:183–207.
- Ebel D. S. and Grossman L. 2000. Condensation in dust-enriched systems. *Geochimica et Cosmochimica Acta* 64:339–366.
- Grossman L. 1972. Condensation in the primitive solar nebula. *Geochimica et Cosmochimica Acta* 36:597–619.
- Grossman L. and Olsen E. 1974. Origin of the high temperature fraction of C2 chondrites. *Geochimica et Cosmochimica Acta* 38:173–187.
- Grossman L. and Steele I. M. 1976. Amoeboid olivine aggregates in the Allende meteorite. *Geochimica et Cosmochimica Acta* 40:149–155.
- Grossman J. N. and Wasson J. T. 1982. Evidence for primitive components in chondrules from the Chainpur chondrite. *Geochimica et Cosmochimica Acta* 46:1081–1099.
- Hashimoto A. and Grossman L. 1987. Alteration of Al-rich inclusions inside amoeboid olivine aggregates in the Allende meteorite. *Geochimica et Cosmochimica Acta* 51:1685–1704.
- Hertz J., Ebel D. S., and Weisberg M. K. 2003. Tomographic study of shapes and metal abundances of Renazzo chondrules (abstract #1959). 34th Lunar and Planetary Science Conference. CD-ROM.
- Hummayun M., Campbell A. J., Zanda B., and Bourot-Denise M. 2002. Formation of Renazzo chondrules metal inferred from siderophile elements (abstract #1965). 33rd Lunar and Planetary Science Conference. CD-ROM.
- Imae N., Tsuchiyama A., and Kitamura M. 1993. An experimental study of enstatite formation reaction between forsterite and Si-rich gas. *Earth and Planetary Science Letters* 118:21–30.
- Joung R. M. K., MacLow M. M., and Ebel D. S. 2004. Chondrule formation and protoplanetary disk heating by current sheets in nonideal magnetohydrodynamic turbulence. *The Astrophysical Journal* 606:532–541.
- Klöck W., Thomas K. L., McKay D. S., and Palme H. 1989. Unusual olivine and pyroxene compositions in interplanetary dust and unequilibrated ordinary chondrites. *Nature* 339:126–128.
- Kornacki A. S. and Wood J. A. 1984. Petrography and classification Ca-Al-rich and olivine-rich inclusions in the Allende CV3 chondrite. Proceedings, 14th Lunar and Planetary Science Conference. *Journal of Geophysical Research* 89:B573–B587.
- Kornacki A. S., Cohen R. E., and Wood J. A. 1983. Petrography and classification of refractory inclusions in the Allende and Mokoia CV3 chondrites. *Memoirs of the National Institute of Polar Research* 30:45–60.
- Komatsu M., Krot A. N., Petaev M. I., Ulyanov A. A., Keil K., and Miyamoto M. 2001. Mineralogy and petrography of amoeboid

- olivine aggregates from the reduced CV3 chondrites Efremovka, Leoville and Vigarano: Products of nebular condensation, accretion, and annealing. *Meteoritics & Planetary Science* 36: 629–641.
- Krot A. N., McKeegan K. D., Leshin L. A., MacPherson G. J., and Scott E. R. D. 2002. Existence of an  $^{16}\text{O}$ -rich gaseous reservoir in the solar nebula. *Science* 295:1051–1054.
- Krot A. N., Petaev M. I., and Yurimoto H. 2003. Low-Ca pyroxene in amoeboid olivine aggregates in primitive carbonaceous chondrites (abstract #1441). 34th Lunar and Planetary Science Conference. CD-ROM.
- Krot A. N., Scott E. D., and Zolensky M. E. 1995. Mineralogic and chemical modification of components in CV3 chondrites: Nebular versus asteroidal processing. *Meteoritics* 30:748–776.
- Krot A. N., Ulyanov A. A., Meibom A., and Keil K. 2001. Forsterite-rich accretionary rims around Ca, Al-rich inclusions from the reduced CV3 chondrite Efremovka. *Meteoritics & Planetary Science* 36:611–628.
- Larimer J. W. 1967. Early condensation history of the solar system. *Geochimica et Cosmochimica Acta* 31:1215–1238.
- Lee M. S., Rubin A. E., and Wasson J. T. 1992. Origin of metallic Fe-Ni in Renazzo and related meteorites. *Geochimica et Cosmochimica Acta* 56:2521–2533.
- McSween H. Y., Jr. 1977a. Petrographic variations among carbonaceous chondrites of the Vigarano type. *Geochimica et Cosmochimica Acta* 41:1777–1790.
- McSween H. Y., Jr. 1977b. Carbonaceous chondrites of the Ornans type: A metamorphic sequence. *Geochimica et Cosmochimica Acta* 41:479–491.
- Murrell M. T. and Burnett D. S. 1987. Actinide chemistry in Allende Ca-Al-rich inclusions. *Geochimica et Cosmochimica Acta* 51: 985–999.
- Nierderer F. R., Papanastassiou D. A., and Wasserburg G. J. 1985. Absolute isotopic abundances of Ti in meteorites. *Geochimica et Cosmochimica Acta* 49:835–851.
- Pouchou J. L. and Pichoir F. 1991. Quantitative analysis of homogeneous or stratified micro-volumes applying the model “PAP.” In *Electron probe quantitation*, edited by Heinrich K. F. J. and Newbury D. E. New York: Plenum Press. pp. 31–75.
- Rubin A. E., James J. A., Keck B. D., Weeks K. S., Sears D. W. G., and Jarosewich E. 1985. The Colony meteorite and variations in CO3 chondrite properties. *Meteoritics* 20:175–196.
- Sack R.O., and Ghiorso M. S. 1994. Thermodynamics of multicomponent pyroxenes III: Calibration of  $\text{Fe}^{2+}(\text{Mg})_{-1}$ ,  $\text{TiAl}(\text{MgSi})_{-1}$ ,  $\text{TiFe}^{3+}(\text{MgSi})_{-1}$ ,  $\text{AlFe}^{3+}(\text{MgSi})_{-1}$ ,  $\text{NaAl}(\text{CaMg})_{-1}$ ,  $\text{Al}_2(\text{MgSi})_{-1}$  and  $\text{Ca}(\text{Mg})_{-1}$  exchange reactions between pyroxenes and silicate melts. *Contributions to Mineralogy and Petrology* 118:271–296.
- Wai C. M. and Wasson J. T. 1977. Nebular condensation of moderately volatile elements and their abundances in ordinary chondrites. *Earth and Planetary Science Letters* 36:1–13.
- Wark D. A. and Lovering J. F. 1977. Marker events in the early solar system: Evidence from rims on Ca-Al-rich inclusions in carbonaceous chondrites. Proceedings, 8th Lunar and Planetary Science Conference. pp. 95–112.
- Weisberg M. K., Ebel D. S., Connolly H. C., Jr., Boesenberg J. S., and Castellano D. 2002. Petrologic-tomographic study of metal in the CR chondrites (abstract). *Meteoritics & Planetary Science* 37: A149.
- Weisberg M. K. and Prinz M. 1990. Refractory-rich inclusions in the CR2 (Renazzo-type) chondrites. 21st Lunar and Planetary Science Conference. pp. 1315–1316.
- Weisberg M. K., Prinz M., Clayton R. N., and Mayeda T. K. 1993. The CR (Renazzo-type) carbonaceous chondrite group and its implications. *Geochimica et Cosmochimica Acta* 57:1567–1586.
- Weisberg M. K., Prinz M., Kennedy A., and Hutcheon I. D. 1991. Trace elements in refractory-rich inclusions in CR2 chondrites. *Meteoritics* 26:407–408.
- Yurimoto H. and Wasson J. T. 2002. Extremely rapid cooling of a carbonaceous chondrite chondrule containing very  $^{16}\text{O}$ -rich olivine and a  $^{26}\text{Mg}$ -excess. *Geochimica et Cosmochimica Acta* 66:4355–4363.
- Zanda B., Bourot-Denise M., Hewins R. H., Cohen B. A., Delaney J. S., Humayun M., and Campbell A. J. 2002. Accretion textures, iron evaporation, and recondensation in Renazzo chondrules (abstract #1852). 33rd Lunar and Planetary Science Conference. CD-ROM.